Annealing-induced full amorphization in a multicomponent metallic film

J. P. Chu,[1] C. T. Liu,[2] T. Mahalingam,[1,*] S. F. Wang,[3] M. J. O'Keefe,[4] B. Johnson,[4] and C. H. Kuo[1]
[1]*Institute of Materials Engineering, National Taiwan Ocean University, Keelung 202, Taiwan, Republic of China*
[2]*Metals and Ceramics Div., Oak Ridge National Laboratory, P.O. Box 2008, Oak Ridge, Tennessee 37831, USA*
[3]*Department of Materials and Minerals Resources Eng., National Taipei Univ. of Tech., Taipei 106, Taiwan, Republic of China*
[4]*Department of Metallurgical Engineering, University of Missouri-Rolla, Rolla, Missouri 65409, USA*
(Received 31 December 2003; published 26 March 2004)

We present direct experimental evidence that controllable amorphization and nanocrystallization during annealing of metastable films could serve as a precursor for exciting nanomaterials. The interesting discovery is that certain sputtered crystalline films become completely amorphous when annealed in the temperature range between the glass temperature and the crystallization temperature. Unlike other metallic glassy materials that exhibit annealing-induced devitrification, our good glass-forming films are transformed into various nanoscale and amorphous structures due to the annealing process. The formation of an amorphous phase gives rise to notable alterations in the electrical and mechanical properties of the film.

DOI: 10.1103/PhysRevB.69.113410 PACS number(s): 61.43.Er, 68.55.Jk, 81.05.Kf, 81.07.Bc

INTRODUCTION

Crystallization generally tends to occur during the thermal annealing of amorphous sputtered films because crystalline phases are more thermodynamically favorable than metastable phases formed in the as-deposited condition.[1] In certain elementally modulated crystalline films, solid-state amorphization (SSA) has been reported to take place through annealing-induced diffusion reactions.[2] However, the extent of amorphization in this case is trivial and confined to the reacted interfacial thickness of typical few nanometers. In the present work, we report extensive amorphization in sputtered films when annealed in the temperature range between the glass temperature and the crystallization temperature. Annealing of sputtered metastable films is found to cause the formation of various nanoscale and amorphous structures, thus resulting in changes of electrical and mechanical properties. The Zr-Cu-Al-Ni alloy is chosen because it is one of the principal bulk metallic glasses (BMGs) revealing good glass-forming ability.[3,4] The recent advent of BMGs with a relatively high thermal stability and low critical cooling rates has attracted great attention to the fundamental and applied research due to their potential use in engineering applications. The research and development of BMGs also make thin film processing possible, which was not readily achieved in the past when metallic glasses were available only in forms of powder and ribbon.

EXPERIMENTAL PROCEDURE

Zr-31Cu-13Al-9Ni (atomic percent, at. %) films of thickness 5–10 μm were deposited onto glass substrates using a rf magnetron sputtering system with a 3-mTorr working pressure and 100-W power. The film was annealed in Ar at a heating rate of 40 K/min and a holding time of 60 s at temperatures ranging from 550 to 950 K. The annealing system was pumped down to the mTorr range followed by several purgings with Ar. To prevent oxidation at high temperatures ($\geqslant$850 K), the films were capped with a ~50-nm-thick sputtered Pt overlay. The thermal behavior of the film was determined using a differential scanning calorimeter (DSC) in Ar at a heating rate of 40 K/min. The DSC film sample was delaminated from the glass without the aid of any chemical solutions. Depth profiles of the oxygen concentration together with other alloying elements present in the film were determined by point analyses with a point-to-point distance of ~1 μm, using the ORNL JEOL Electron Superprobe at 15 keV. Films with substrates were mounted at a taper angle of 45° to expand the exposure of film thickness by ~41% for chemical analyses. Plane-view transmission electron microscopy (TEM) analyses of the films were done using Philips EM 430T at 300 keV. The specimens were prepared using mechanical polishing, dimpling, and ion milling from the backside of the sample to remove the substrate for the final perforation of the film. For the capped films, the Pt was completely removed by ion polishing as confirmed by an x-ray energy dispersive spectroscopy analysis. Sheet resistance and hardness measurements were performed on the films without the Pt overlay by four-point probe and Knoop ultramicrohardness methods, respectively. The ultramicrohardness was measured with a 25-g loading, a 15-s holding time, and a loading rate of 40 μm/s.

RESULTS

The DSC result in Fig. 1(a) shows that the as-deposited film underwent a glass transition (T_g) and crystallization (T_x) at 758.3 and 797.2 K, respectively. The supercooled liquid region (ΔT), defined as the difference between T_g and T_x, is thus measured to be ~39 K. This value is in the range reported for sputtered Pd-17Si-7Cu (Ref. 5) and Zr-19Cu-6Al (Ref. 6) films, even though there are differences in the experimental apparatus and heating rate conditions between this work and those studies. Based on the DSC result, an annealing of films at different temperatures was performed. As will be shown, the annealing of films yields different structures that leads to variations in film properties. Annealing at temperatures well below T_g resulted in a decrease in the film hardness, as seen in Fig. 1(b). Above 550 K, the film hardness gradually increased with increasing temperature,

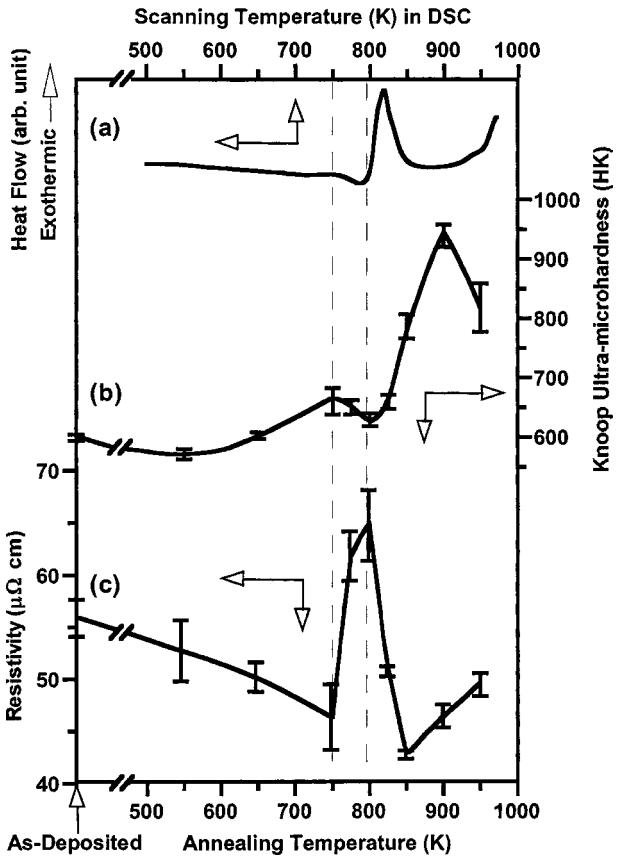

FIG. 1. (a) A DSC thermogram of an as-deposited film; variations of (b) the Knoop ultramicrohardness and (c) the electrical resistivity with the annealing temperature. The approximate location of supercooled liquid region is marked by dash lines to facilitate visual comparison.

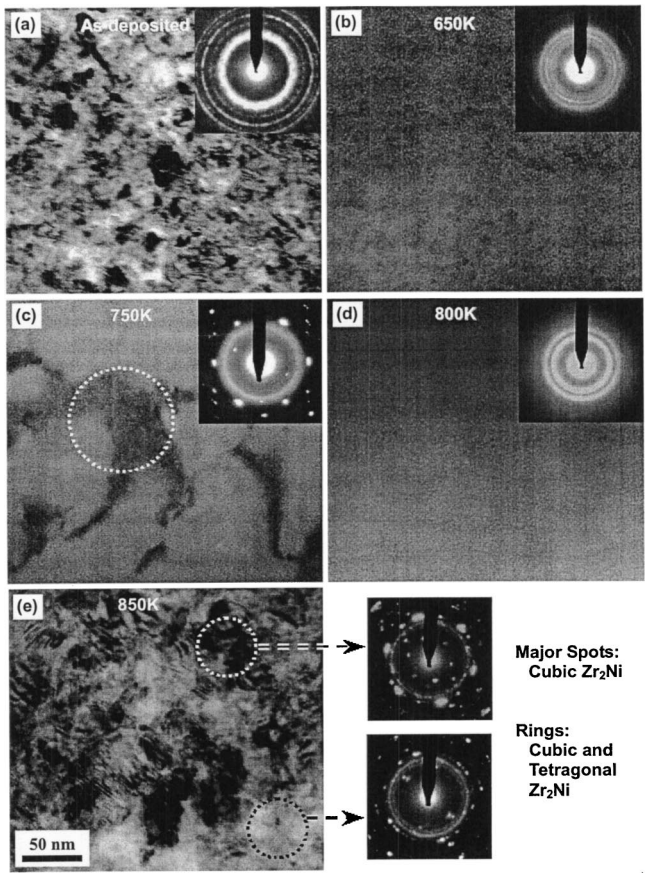

FIG. 2. Plane-view TEM micrographs and diffraction patterns of the films in (a) as-deposited and annealed conditions at (b) 650, (c) 750, (d) 800, and (e) 850 K. The circled regions indicate the locations for obtaining the diffraction patterns.

reaching a maximum of ~HK670 at 750 K. When annealed at 800 K, within ΔT, the film hardness decreased slightly to ~HK630. For temperatures above T_x, the hardness increased sharply to a maximum value of ~HK945 at 900 K, a ~60% increase than measured for the as-deposited film. With the exception of the decrease in ΔT, the film hardness reveals an increasing trend with temperature. Unlike other sputtered metastable films showing a negative temperature dependence on the film hardness,[7,8] our films showed an increasing trend in hardness with annealing temperature. This beneficial strengthening behavior may be a characteristic of annealed metallic glass thin films, which could lead to a class of high performance materials. In Fig. 1(c), an abrupt increase (~40%) in the film resistivity to ~65 $\mu\Omega$ cm at 800 K is noted for the film annealed in ΔT. Annealing at temperatures below T_g resulted in a decrease in the film resistivity, to ~46 $\mu\Omega$ cm at 750 K. In general, a decreasing trend of the film resistivity with the temperature was observed except for a dramatic increase in ΔT. When compared with that of sputter deposited Pd-based glass-forming alloy films, a similar increase in film resistivity near T_g has been reported.[5] However, due to the lack of crystal structure/microstructure details and resistivity values in ΔT,[5] it is inconclusive to determine whether full amorphization in the Pd-based films occurred.

The TEM image and the associated diffraction ring pattern of the as-deposited film in Fig. 2(a) clearly indicate a typical sputtered nanocrystalline structure. The nanocrystallites have sizes in the range of 10–30 nm. According to the diffraction pattern, the structure is either tetragonal Zr_2Ni (JCPDS 38-1170) or cubic Zr_2Ni (JCPDS 41-0898). After annealing at 650 K, the microstructure has transformed into a two-phase nanophase composite of an amorphous matrix containing uniformly dispersed nanocrystallites [Fig. 2(b)]. The refined crystallites are ~10–20 nm in diameter. Even though it is difficult to observe in the micrograph, continuous, diffuse diffraction ring pattern suggests that the film consists of finer crystallites than those present in the as-deposited condition. When annealed at 750 K, about the onset of T_g, the agglomeration and growth of nanocrystalline phases in the form of crystalline networks embedded in an amorphous matrix are seen in Fig. 2(c). The diffraction pattern from the area highlighted by the circle was a spot pattern indicative of crystallized Zr_3Al and Ni_7Zr_2 phases. The existence of nanometer-sized crystalline phases is unique and could explain why the film hardness increased and the resistivity decreased at 750 K. The hardness increase is thus thought to be caused by a so-called nanophase composite structure, and such a strengthening effect is analogous to that reported in many partially-crystallized BMGs prepared by

casting or by an annealing-induced devitrification of amorphous materials.[3,9] Surprisingly, annealing at 800 K, in ΔT, produced a fully amorphous structure. No crystalline phases were observed in the TEM image and the broad, diffuse diffraction rings were seen [Fig. 2(d)]. The presence of this distinct, amorphous structure can explain the drop in hardness and increase in resistivity measured at 800 K. The film annealed at 850 K, above T_x, did crystallize into nanocrystalline phases and substantial crystallized regions were observed in the diffraction patterns [Fig. 2(e)]. The crystalline phases are identified to be predominately cubic and tetragonal Zr_2Ni.

DISCUSSION

Hydrogen has been reported to induce amorphization in many alloys under highly pressurized ($\sim$5 MPa) and elevated temperature environments.[10] Such a possibility is unlikely in this study because the short annealing duration and reduced pressure are unfavorable to allow hydrogen diffusion to occur. Oxygen impurity and contamination are known to strongly affect the stability of the amorphous phase in BMGs.[11,12] As Zr and its alloys are known to be susceptible to oxidation, incorporation of oxygen into the film is often very difficult to avoid even in the reduced and protective annealing environment. However, the oxygen effect would be negligible for the annealing temperatures $\leqslant$800 K on account of the following reasons. The interaction of Zr with oxygen involves both oxygen dissolution and formation of scale (mainly ZrO_2).[13] The scale formation was limited in this study because our x-ray diffraction analysis results (which are not shown here) revealed the presence of oxide phases only at and above 850 K. The oxygen dissolution during annealing is thus considered in this study. In the absence of an exact diffusion coefficient D, we take an Arrhenius expression, $D(\text{in cm}^2/\text{sec}) = 5.2\exp[-212/(8.314\cdot T)]$, where T is absolute temperature. This expression has been commonly used for Zr and its alloys to determine the depth of oxygen dissolved into the metal through volume diffusion.[13] Based on $X = 2\sqrt{Dt}$, where t is the annealing time and X the distance at which the oxygen concentration falls to half the initial value of maximum solubility (28.5%) at the metal oxide interface,[13] and an assumption that the time spent in heating up to 0.8 of annealing temperature makes insignificant contributions to the total amount of diffusion,[14] depths of oxygen dissolution into our annealed films are estimated to be 0.1, 0.3, 0.7, and 1.4 μm for 800, 850, 900, and 950 K, respectively. The estimate is consistent with the depth profile of oxygen concentration shown in Fig. 3. This figure indicates no oxygen contamination due to annealing at 800 K. The average oxygen content in the as-deposited film is, within the experimental error, nearly equal to that of the sample annealed at 800 K. Based on this comparison, we conclude that the formation of amorphous phase during the 800 K annealing is not associated with oxygen contamination at all.

Upon annealing, our films clearly show a structure development sequence of metastable sputtered structure $\rightarrow$metastable nanocrystallite/amorphous nanophase composite$\rightarrow$single metastable amorphous phase$\rightarrow$stable crystalline structure. While the amorphization mechanism in this study might not be the same, the amorphization of metals during heating has been reported in a metastable high-pressure crystalline Cd-Sb alloy[15] and a supersaturated crystalline Ti-Cr alloy[16] in which intermediate metastable amorphous phases with lower free energies were formed before equilibrium phases were developed. To interpret the present results and explain the thermodynamics that govern the structure evolution during annealing, hypothetical free-energy diagrams are shown in Fig. 4. The diagrams, though approximate, contain the essential features required to interpret the present results. The relative position of the free energy curves in the figure is rationalized based on thermodynamic considerations. In this figure, of primary importance is the large negative heat of mixing observed for the Zr-based alloy system.[4] Inoue has suggested that the large negative heat of mixing enables multicomponent alloys to readily form a glassy phase during cooling from the melt.[4] The large negative heat of mixing and hence the low free energy of the amorphous phase can be related to the amorphization in our case. The low free energy serves as the thermodynamic driving force for the amorphous phase to form as an intermediate phase during annealing, which eventually becomes thermodynamically stable by complete crystallization at high temperatures. Based on the schematic, it is anticipated that a similar amorphization behavior could take place in other sputtered glass-forming films with large negative heat formation.

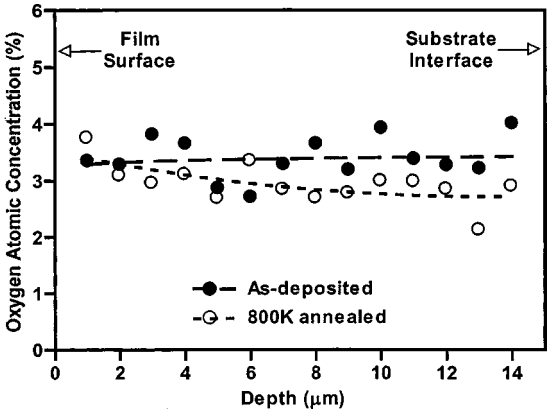

FIG. 3. Depth profiles of oxygen concentration in uncapped films in as-deposited and 800-K-annealed conditions obtained by point analyses. Average oxygen concentrations in atomic percent are 3.40 ± 0.37 and 2.96 ± 0.36 for as-deposited and 800-K-annealed films, respectively.

In addition to the thermodynamic factor, the thermal energy at elevated temperatures and the interfacial energy arising from the nanocrystallite/glass interfaces are kinetically favorable for the amorphization, as proposed previously in SSA.[17] At low temperatures, the large interfacial energy drives coarsening of the metastable crystalline phase through a process analogous to Ostwald ripening, and the nanocrystallites become interconnected to form a network structure. Once this interconnected crystalline network structure is formed, facilitating the flow of electrical current, a decrease

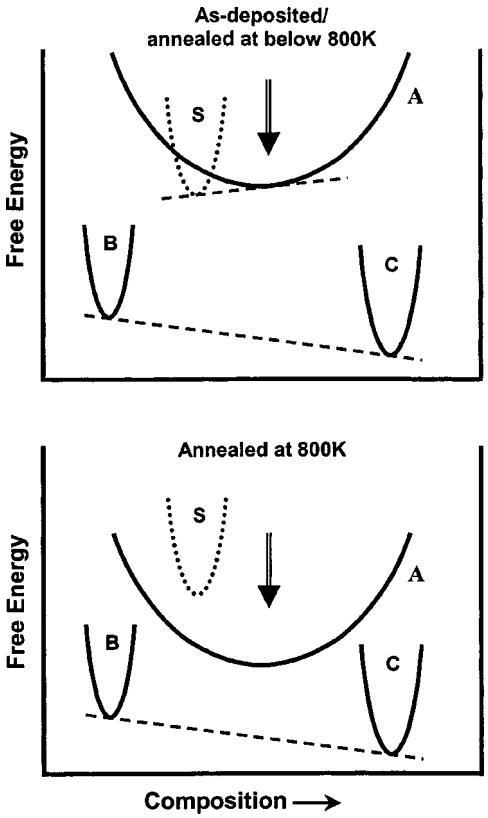

FIG. 4. A schematic illustration showing the free energy relationship between the metastable sputtered phase (S), amorphous phase (A), and stable crystalline phases (B and C) in the films annealed at low temperatures and 800 K. The arrows indicate the film composition.

in resistivity is resulted. Further, the viscosity of the glass matrix presumably decreases with temperature, analogous to that required for the superplasticity behavior of metallic glasses.[18] The glassy matrix, with a sufficiently low viscosity, allows the metastable nanocrystalline phases to ''move around'' and reorient in the matrix. In ΔT, a complete amorphization occurs as the metastable nanocrystallites are thermally annihilated and ''liquefied'' into the glassy matrix due to the combined effects of sufficient thermal energy and excessive interfacial energy. In contrast to the planar interfacial area in SSA multilayer films, the single layer films in this study are considered to yield much higher interfacial energies since nanocrystallite/glass interfaces are present through the film thickness. As a result, wide spread amorphization could take place in the film. Above T_x, the amorphous structure is no longer thermodynamically favorable and crystallization readily proceeds.

CONCLUSIONS

The present work provides direct experimental evidence that annealing of Zn-31Cu-13Al-9Ni films results in nanocrystallization and amorphization. The amorphization takes place presumably due to the low free energy of the amorphous phase with sufficient thermal and interfacial energies between nanocrystallites and a glassy matrix. The formation of a comprehensive amorphous structure gives rise to notable alterations in the electrical and mechanical properties of the annealed film. Additional features of this work are that a profound strengthening effect is observed and that one can take this advantage to *tailor* the film properties by modulating the amorphous content in the annealed films.

ACKNOWLEDGMENTS

This work was funded by the National Science Council of the Republic of China (91-2216-E-019-004) and by the Division of Materials Science and Engineering, Office of Basic Energy Sciences, U.S. Department of Energy, under Contract No. DE-AC05-00OR22725 with UT-Battelle, LLC. The authors are grateful to J. R. Walker, Y. L. Lin, R. R. Jeng, C. T. Lo, and P. Y. Lee, W. Kai and C. Robert Kao for their contributions.

*Permanent address: Department of Physics, Alagappa University, Karaikudi-630 003, India.

[1] J. P. Chu, S. F. Wang, S. J. Lee, and C. W. Chang, J. Appl. Phys. **88**, 6086 (2000).
[2] R. B. Schwarz and W. L. Johnson, Phys. Rev. Lett. **51**, 415 (1983).
[3] A. L. Greer, Science **267**, 1947 (1995).
[4] A. Inoue, Acta Mater. **48**, 279 (2000).
[5] Y. Liu, S. Hata, K. Wada, and A. Shimokohbe, Jpn. J. Appl. Phys. **40**, 5382 (2001).
[6] S. Hata, Y. Liu, T. Kato, and A. Shimokohbe, *Proceedings of the International Conference on Precision Engineering* (The Japan Society for Precision Engineering, Tokyo, Japan, 2001), pp. 37–41.
[7] J. P. Chu, C. H. Chung, P. Y. Lee, J. M. Rigsbee, and J. Y. Wang, Metall. Mater. Trans. A **29A**, 647 (1998).
[8] J. P. Chu and T. N. Lin, J. Appl. Phys. **85**, 6462 (1999).
[9] A. Inoue, Mater. Sci. Eng., A **304-306**, 1 (2001).
[10] X. L. Yeh, K. Samwer, and W. L. Johnson, Appl. Phys. Lett. **42**, 242 (1983).
[11] C. T. Liu, M. F. Chisholm, and M. K. Miller, Intermetallics **10**, 1105 (2002).
[12] D. J. Sordelet, X. Y. Yang, E. A. Rozhkova, M. F. Besser, and M. J. Kramer, Appl. Phys. Lett. **83**, 69 (2003).
[13] A. S. Khanna, *Introduction to High Temperature Oxidation and Corrosion* (ASM International, Materials Park, OH, 2002), pp. 101–103.
[14] P. G. Shewmon, *Diffusion in Solids* (Minerals, Metals & Materials Society, Warrendale, PA, 1989), pp. 37–38.
[15] N. V. Alekseechkin, A. S. Bakai, and C. Abromeit, J. Phys.: Condens. Matter **13**, 7223 (2001).
[16] A. L. Greer, J. Less-Common Met. **140**, 327 (1988).
[17] Z. F. Li, W. S. Lai, and B. X. Liu, Appl. Phys. Lett. **77**, 3920 (2000).
[18] J. P. Chu, C. L. Chiang, T. Mahalingam, and T. G. Nieh, Scr. Mater. **49**, 435 (2003).